Aeolian Research 23 (2016) 1–10

Contents lists available at ScienceDirect

Aeolian Research

journal homepage: www.elsevier.com/locate/aeolia

The formation of snow streamers in the turbulent atmosphere boundary layer

Ning Huang, Zheng-Shi Wang *

Key Laboratory of Mechanics on Disaster and Environment in Western China (Lanzhou University), The Ministry of Education of China, 730000, China
Department of Mechanics, School of Civil Engineering and Mechanics, Lanzhou University, Lanzhou, 730000, China

ARTICLE INFO

Article history:
Received 20 March 2016
Revised 9 September 2016
Accepted 9 September 2016

Keywords:
Drifting snow
Large Eddy Simulation (LES)
Turbulent boundary layer
Snow streamers

ABSTRACT

The drifting snow in the turbulent atmosphere boundary layer is an important type of aeolian multi-phase flow. Current theoretical and numerical studies of drifting snow mostly consider the flow field as steady wind velocity. Whereas, little is known about the effects of turbulent wind structures on saltating snow particles. In this paper, a 3-D drifting snow model based on Large Eddy Simulation is established, in which the trajectory of every snow grain is calculated and the coupling effect between wind field and snow particles is considered. The results indicate that the saltating snow particles are reorganized by the suction effect of high-speed rotating vortexes, which results in the local convergence of particle concentration, known as snow streamers. The turbulent wind leads to the spatial non-uniform of snow particles lifted by aerodynamic entrainment, but this does not affect the formation of snow streamers. Whereas the stochastic grain-bed interactions make a great contribution to the final shapes of snow streamers. Generally, snow streamers display a characteristic length about 0.5 m and a characteristic width of approximately 0.16 m, and their characteristic sizes are not sensitive to the wind speed. Compared to the typical sand streamer, snow streamer is slightly narrower and the occurrence of other complex streamer patterns is later than that of sand streamers due to the better follow performance of snow grains with air flow.

1. Introduction

Drifting snow is a typical two-phase flow that frequently occurred at high latitudes and its studies are of glaciological and hydrological importance (Zhou et al., 2014). The drifting snow process carries snow grains from one place to another and results in a redistribution of snow cover. On one hand, the non-uniform distribution snow layer caused by drifting snow on mountains may induce and aggravate various natural geologic hazards (Michaux et al., 2001). On the other hand, drifting snow is one of the main causes of the temporal and spatial variation of snow distribution, contributes greatly to the mass balance of the ice sheets (Gallée et al., 2013). Thus, the dispersion and transport characteristics of snow particles in the turbulent boundary layer require in-depth research.

Many drifting snow models have been proposed to investigate this comprehensive phenomenon. Most of them are two-fluid models assume snow particles a continuous phase (Uematsu et al., 1991; Mann et al., 2000; Taylor, 1998; Déry and Yau, 1999; Fukushima et al., 1999, 2001; Xiao et al., 2000; Bintanja, 2000a, 2000b; Gauer, 2001; Lehning et al., 2008; Schneiderbauer and Prokop, 2011; Vionnet et al., 2014). These models have greatly improved our understanding of drifting snow process. However, snow grains can also saltate downflow due to the gravitational effect. The movement of mid-air snow particles and the interaction between snow grains and turbulent structures are essential for understanding the natural drifting snow process and its spatial structure under the action of turbulent wind. In recent years, some Euler-Lagrange models have been explored to investigate the drifting snow process, in which the snow particles were tracked with Lagrange method. Nemoto and Nishimura (2004) studied 2-D snow particle motions in the 1-D turbulent boundary layer based on particle tracking with consideration of the aerodynamic entrainment and wind modification. Later, Zhang and Huang (2008) presented a steady state snow drift model and analyzed the features of the steady state of drifting snow.

The studies on the dispersion of solid particles in the 3-D turbulent boundary layer based on Large Eddy Simulation (LES) have also been conducted by researchers. Vinkovic et al. (2006) studied

* Corresponding author at: Key Laboratory of Mechanics on Disaster and Environment in Western China (Lanzhou University), The Ministry of Education of China, 730000, China.
E-mail address: wangzhsh2013@lzu.edu.cn (Z.-S. Wang).

http://dx.doi.org/10.1016/j.aeolia.2016.09.002
1875-9637/

the dispersion of solid particles in a turbulent boundary layer based on the large-eddy simulation combined with the dynamic Germano subgrid-scale (SGS) model, while the spatial structure of the sand flow was not discussed. Then, Dupont et al. (2013) simulated the wind-blown sand movement in the near surface turbulent flow layer and found the process of sand saltation is very intermittent in time and space due to the turbulence of the flow. Groot Zwaaftink et al. (2014) simulated the small-scale drifting snow in the turbulent boundary layer and analyzed the intermittency of drifting snow by simplifying the coupling effect between particles and wind field as a uniform roughness modification. This may be inaccurate since the saltating snow particles are non-uniform distributed in the turbulent flow. Huang and Wang (2015) performed the behaviors of snow particle in a fully developed turbulent boundary layer and snow streamers were reproduced. Up to now, the characteristic sizes of snow streamer and its formation mechanisms require further exploration. In addition, all above studies didn't adopt an adequate SGS model to reflect the influence of non-uniform distributed saltation particles on the wind field, which will affect the final structure of the drifting snow to a great extent.

Here, we investigate the influence of turbulent structures on saltating snow using a Lagrangian dynamic subgrid-scale (SGS) model (Meneveau et al., 1996). This model averages the Smagorinsky coefficient in time following fluid pathlines and can match the non-uniform drag force due to the saltating snow particles essentially. The coupling effect between snow particles and wind field is explicitly considered. Each saltating snow particle is tracked using a Lagrangian approach and a splash scheme is used to describe the grain-bed interactions. The development of drifting snow in the turbulent boundary layer with mixed grain size is numerically studied and 'snow streamers' in the turbulent boundary layer are reproduced. The most important improvement of this model is that the reaction force of each saltating particle is calculated and imposed on the wind field and each single particle is tracked separately in order to obtain the detail structure of blown snow in the turbulent boundary layer. The spatial distribution characteristic of snow streamers and its relevance with turbulent wind structure are analyzed in detail.

2. Model and methods

2.1. Turbulent boundary layer

The ARPS (Advanced Regional Prediction System, version 5.3.3) developed by University of Oklahoma is a middle-scale meteorological model, and the three-dimensional, non-hydrostatic, compressible Navier-Stokes equation is solved using the 'split-explicit' time integration method (Xue et al., 2000, 2001). After introduce the reaction force of saltating snow particles into the Navier-Stokes equation, the fluid governing equations can be expressed as:

$$\frac{\partial \rho}{\partial t}+\frac{\partial}{\partial x_i}(\rho \bar{u}_i)=0 \tag{1}$$

$$\frac{\partial}{\partial t}(\rho \bar{u}_i)+\frac{\partial}{\partial x_j}(\rho \bar{u}_i \bar{u}_j)=-\left(\frac{\partial \overline{p^*}}{\partial x_i}+g\frac{\rho'}{\rho}\right)-\frac{\partial \tau_{ij}}{\partial x_j}-F_i \tag{2}$$

where the line symbol indicates the filtered variables. $x_i(m)$ is the position coordinates and $i=1,2,3$ stand for the streamwise, lateral, and vertical directions, respectively; u_i (ms^{-1}) refers to the instantaneous velocity component of three directions, t (s) is time, $p^*=p'-\alpha\nabla(\bar{\rho}\mathbf{u})$ (Nm^{-3}) contains the pressure perturbation and a divergence damping terms, the ρ' and ρ $(\mathrm{Kg\,m}^{-3})$ are the perturbance density and grid-averaged density of air, respectively; g (ms^{-2}) is the gravitational acceleration, and $\tau_{ij}=\rho\overline{u_i u_j}-\rho\bar{u}_i\bar{u}_j$ is the subgrid stress, according to Smagorinsky (1963):

$$\tau_{ij}=-2(C_s\Delta)^2|\bar{S}|\bar{S}_{ij} \tag{3}$$

where Δ (m) is the filter scale, $\bar{S}_{ij}=(\partial\bar{u}_i/\partial x_j+\partial\bar{u}_j/\partial x_i)/2$ is the strain rate tensor, and C_s is the Smagorinsky coefficient, which is dynamically determined according to the Lagrangian dynamic SGS model (Meneveau et al., 1996).

F_i is the reaction force per unit volume of saltating particles and should be equal and opposite in direction of the drag force of snow particle (Anderson and Haff, 1991):

$$F_i=\frac{1}{V_{grid}}\sum_{s=1}^{N}\frac{3}{4}m_p C_D V_{ri}^2/d_p \tag{4}$$

where V_{grid} (m^3) is the volume of grid cell, N is the total number of particles in a grid, m_p (kg) means the mass of particles, C_D is the drag coefficient and V_r (ms^{-1}) represents the relative velocity between the particle and air flow.

2.2. Governing equation of particle motion

The Lagrangian Particle Tracking Method combined with fourth order Ronge-Kutta method is used to track the snow grains. As the particle density ρ_p is much larger than the air ($\rho_p=912\ kgm^{-3}$ and $\rho=1.225\ kgm^{-3}$) and its diameter d_p (m) is much smaller than the Kolmogorov scale, every snow particle is regarded as a sphere and only possesses gravity and drag force (Anderson and Haff, 1988). The static electric force is not included in this simulation. Thus, the equation of particle motion can be written as:

$$\frac{du_{pi}}{dt}=\frac{3\rho\mu V_{ri}}{4\rho_p(d_p)^2}C_D Re_p+g_i\left(1-\frac{\rho}{\rho_p}\right) \tag{5}$$

$$C_D Re_p=\begin{cases}24+3.6(Re_p)^{0.687},(Re_p\leqslant 1000)\\ 0.44Re_p,(Re_p>1000)\end{cases} \tag{6}$$

where $Re_p=d_pV_r/v$ is the particle Reynolds number and $v=1.5\times10^{-5}\ \mathrm{m^2\ s^{-1}}$ is the kinematic viscosity of air.

2.3. Grain-bed interactions

Snow particles will be entrained into the air if the shear force generated by air flow is above threshold. The aerodynamic entrainment scheme of Groot Zwaaftink et al. (2014) is adopted to describe the quantity and initial velocities of entrained particles.

When a moving particle impacts on the bed, it may rebound into air again and eject new particles into the air due to momentum transfer. The rebound probability can be expressed as (Anderson and Haff, 1991):

$$P_{reb}=B[1-exp(-\gamma v_{imp})] \tag{7}$$

where $v_{imp}(\mathrm{ms}^{-1})$ is the impact velocity of particle, $B=0.9$ and $\gamma=2\ sm^{-1}$ are empirical parameters (Groot Zwaaftink et al., 2014).

The number of newly ejected particles can be expressed as (Kok and Renno, 2009):

$$N_{ej}=\frac{a}{\sqrt{gD}}\frac{m_{imp}}{\langle m_{ej}\rangle}v_{imp} \tag{8}$$

where a is a dimensionless constant in the range of 0.01–0.05. A value of $a=0.03$ is in accordance with the observation of drifting snow in the wind tunnel (Okaze et al., 2012). D (m) is the typical particle size ($\langle d_p\rangle$ in this paper), m_{imp} (kg) is the mass of impacting particle and $\langle m_{ej}\rangle$ (kg) is the average mass of ejection grains.

According to Kok and Renno (2009), the fraction of kinetic energy retained by the rebounding particle is $(45 \pm 22)\%$ and the speed of the ejected particles is exponentially distributed:

$$\frac{\langle v_{ej}\rangle}{\sqrt{gD}} = \frac{\langle \lambda_{ej}\rangle}{a}\left[1 - \exp\left(-\frac{v_{imp}}{40\sqrt{gD}}\right)\right] \tag{9}$$

where $\langle \lambda_{ej}\rangle = 0.15$ is the average fraction of impacting momentum applied on the ejecting surface grains (Rice et al., 1995). The velocity of every new ejected particle will multiply a coefficient that equal to $m_{ej}/\langle m_{ej}\rangle$ in consideration of the overall momentum conservation.

The angle toward the surface of rebounding particles α_{reb} and splashing particles α_{ej} approximately follow an exponential distribution. Whereas the mean values are very different, the angle α_{ej} has a mean value of 50° (Groot Zwaaftink et al., 2014; Kok and Renno, 2009) and the mean value of α_{reb} depends on the particle size (Rice et al., 1995; Li and Zhou, 2007):

$$\langle \alpha_{reb}\rangle = 161.46e^{-\frac{d_p}{250\times 10^{-6}}} + 0.15 \tag{10}$$

Additionally, the angle toward a vertical plane in the streamwise direction β_{hor} of rebounding and splashing particles follow a normal distribution with the mean value of $\langle \beta_{hor}\rangle = 0°$. The variance $\sigma(\beta_{hor})$ was set as 15° after Dupont et al. (2013).

2.4. Simulation details

The computational region is set as $10.0\,\mathrm{m} \times 10.0\,\mathrm{m} \times 5.0\,\mathrm{m}$ with uniform grid of $\Delta x = \Delta y = 0.05$ m in the horizontal direction and the average mesh size of $\Delta z = 0.05$ m in the vertical direction. The vertical grid is stretched by cubic function to acquire detailed information of the surface layer and the smallest grid is $\Delta z_{min} = 0.005$ m. The large time step is 2.0e−4 s and the small time step used to calculate the acoustic wave terms is 2.0e−5 s. In order to generate the turbulent boundary layer, the standard logarithmic profile with random perturbation is used to initialize the wind field and the compressible flow turbulent inflow condition proposed by Urbin and Knight (2001) is applied at the first stage of simulation. The surface roughness that is used to set the initial wind profile is $\langle d_p\rangle/30$ (Bagnold, 1973) and the surface friction is included through applying an extra force $\tau_{ij}A_{cij}$ on the bottom of the first level grid, in which τ_{ij} (Nm^{-2}) is the local shear force and A_{cij} (m^2) is the area of the grid cell at coordinate position (i,j).

The turbulent flow development time is $100 * \delta/U_e$ as Lund et al. (1998) suggested, where δ (m) is the depth of the boundary layer and U_e (ms^{-1}) is the free stream velocity. Particles will take off when the turbulent boundary layer is fully developed. The periodic boundary condition is used when the turbulent boundary layer is fully-developed because the particles conduct periodic boundaries in the computation domain in order to form a spatial development drifting snow. Additionally, the free slip boundary condition and the surface friction is applied at the bottom, which is similar to the semi-slip boundary condition of Xue et al. (2000), and the zero pressure gradient boundary condition combined with a Rayleigh damping layer (1.5 m) are used in the top.

The actual computation time of drifting snow is 60 s, in which a loose snow layer is set on the ground. The size of snow particles on the bed is gamma distributed according to Schmidt (1984) and a random value will be given to each ejected particle:

$$f(d_p) = \frac{d_p^{(\alpha-1)}}{\beta^{\alpha}\Gamma(\alpha)}\exp(-d_p/\beta) \tag{11}$$

where α and β are the shape and scale parameters with value setting as 4.65 and 75.27, respectively, which is in consistence with the observational results of the natural snow (Omiya et al., 2011).

The fundamental purpose of this drifting snow model is to explore the influence of turbulent on the saltating particles and the relationship between the spatial structures of drifting snow and turbulent flow.

3. Results and discussion

3.1. The model validation

First of all, the snow transport flux of drifting snow is obtained through a temporal and spatial averaging of the saltation mass flux at different heights. Fig. 1 illustrates the snow transport rate of unit width versus friction velocity and the snow transport rate per unit area along height. Here, the friction velocity is the pure flow friction velocity and evaluated from the averaged wind profile. It can be observed from Fig. 1(a) that the snow transport flux per unit width increases with an increase in friction velocity, in accordance with the experimental observations of Sugiura et al. (1998). The minute difference mainly comes from the lack of suspended snow due to diffusion process. The distribution of snow transport rate per unit area along height, as shown in Fig. 1(b), also agrees with the experiment data well.

Fig. 2(a) shows the variations of the mean horizontal velocity of snow particles versus height under different friction velocities. And the simulated results are compared with that of the experiment data. From Fig. 2(a), it can be seen that the mean velocity of snow particles is increased with height, which is supported by a series of measurement (Tominaga et al., 2013; Nishimura et al., 2014). Fig. 2 (b) gives the distributions of saltation particle velocities under different wind speeds. It can be seen that the particle velocities along streamwise obey the unimodal distribution, which is not sensitive to the friction velocity. The standard variances of particle velocity under friction velocities of $0.302\,\mathrm{ms}^{-1}$, $0.411\,\mathrm{ms}^{-1}$ and $0.468\,\mathrm{ms}^{-1}$ are 1.38, 1.27 and 1.32, respectively. This also agrees well with the experimental measurement of Nishimura et al. (2014).

Furthermore, the particle size distributions at different heights are given in Fig. 3(a). The friction velocity is $0.302\,\mathrm{ms}^{-1}$ and the statistical interval is 3 cm along height. It can be seen that the particle size distributions are basically not changed with height except that the larger particles partly decrease with the increment of height. Fig. 3(b) shows the variations of mean particle diameter along height under different friction velocities and they are compared with the wind tunnel experiment results of Gromke et al. (2014) and field observations of Gordon and Taylor (2009). It can be seen that the average particle size along height is almost constant in the saltation layer, which agrees well with the measurement data. The mean particle size trends to decrease with height above the saltation layer. This is mainly because the smaller particles are easier to be carried into the suspension layer by the turbulence. And the mean particle size distribution along height is generally not sensitive to the wind speed.

3.2. The snow streamers

Fig. 4(a) shows the color map of the streamwise wind speed of a fully-developed turbulent boundary layer, in which three horizontal slices at different heights (0.01 m, 0.05 m and 0.1 m) are displayed below. The free stream velocity is $10\,\mathrm{ms}^{-1}$. Seen from the horizontal slices at different heights, the streamwise wind speed increases with height on the whole. However, the local wind speed varies considerably at the same height due to the turbulent fluctuations.

The local surface shear force can be obtained by the local friction velocity u_* through the expression $\tau = \rho u_*^2$, in which u_* is cal-

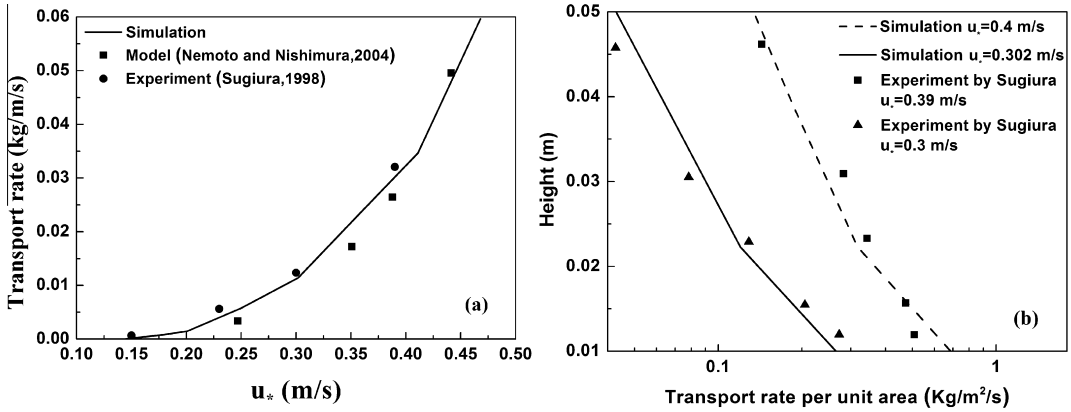

Fig. 1. (a) The snow transport flux versus friction velocity and (b) the snow transport rate per unit area along height.

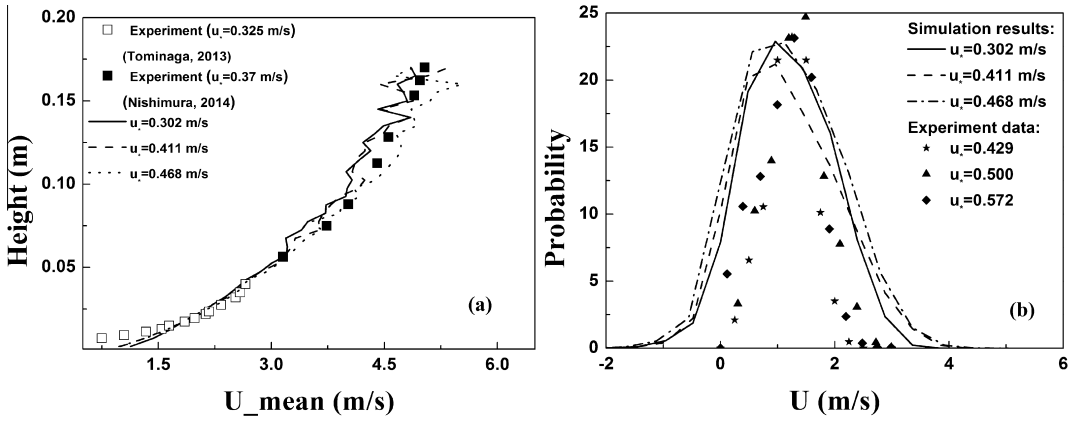

Fig. 2. (a) The mean streamwise velocity of mid-air snow particle along height and (b) the corresponding probability distribution.

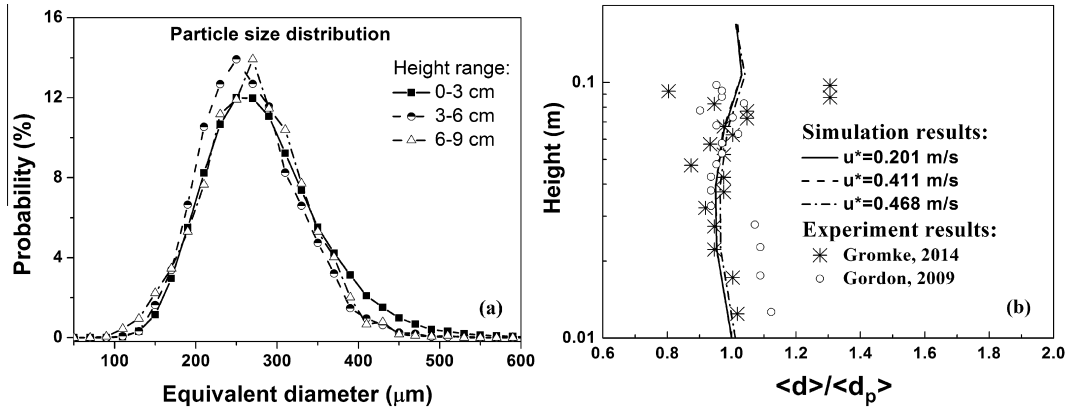

Fig. 3. (a) The particle size distributions at different heights and (b) the comparison between simulated mean particle diameter and experiment results along height.

culated by the wind speed at a height of 0.005 m and the wind profile is assumed to be logarithmic distributed. The surface shear force in a well-developed turbulent boundary layer is displayed in Fig. 3(b) and the free stream velocity is also 10 ms^{-1}. As shown in the figure, very similar to the distribution of wind speed at the near surface, the surface shear force varies greatly and the maximum may be times higher than the minimum. As the aerodynamic entrainment is directly related to the local shear force (Groot Zwaaftink et al., 2014), the number of entrained particles at different positions of the surface may be quite different, and at some places particle even cannot be taken off from the surface. In this way, the initial take-off snow particles will exhibit a quite non-uniform distribution, as shown in Fig. 5(a).

Under the combined action of aerodynamic entrainment and grain-bed interactions, a well-developed drifting snow in equilibrium with the flow is formed in the turbulent boundary layer. Very similar to the observation of Baas (2008) and the simulation of Dupont et al. (2013), the non-uniform distributed saltating particles form the so called 'snow streamer' in the turbulent boundary layer (Huang and Wang, 2015), as shown in Fig. 5(b) and (c). Snow streamers display elongated structure and may merge or bifurcate as they move along the downwind direction (Baas and Sherman, 2005;

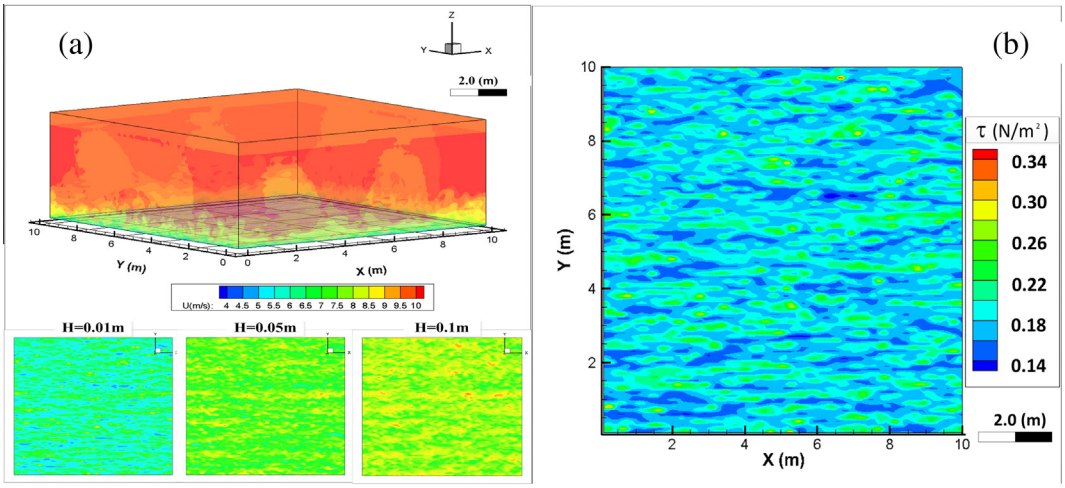

Fig. 4. (a) The color map of streamwise wind speed and (b) the surface shear force in a fully-developed flow field.

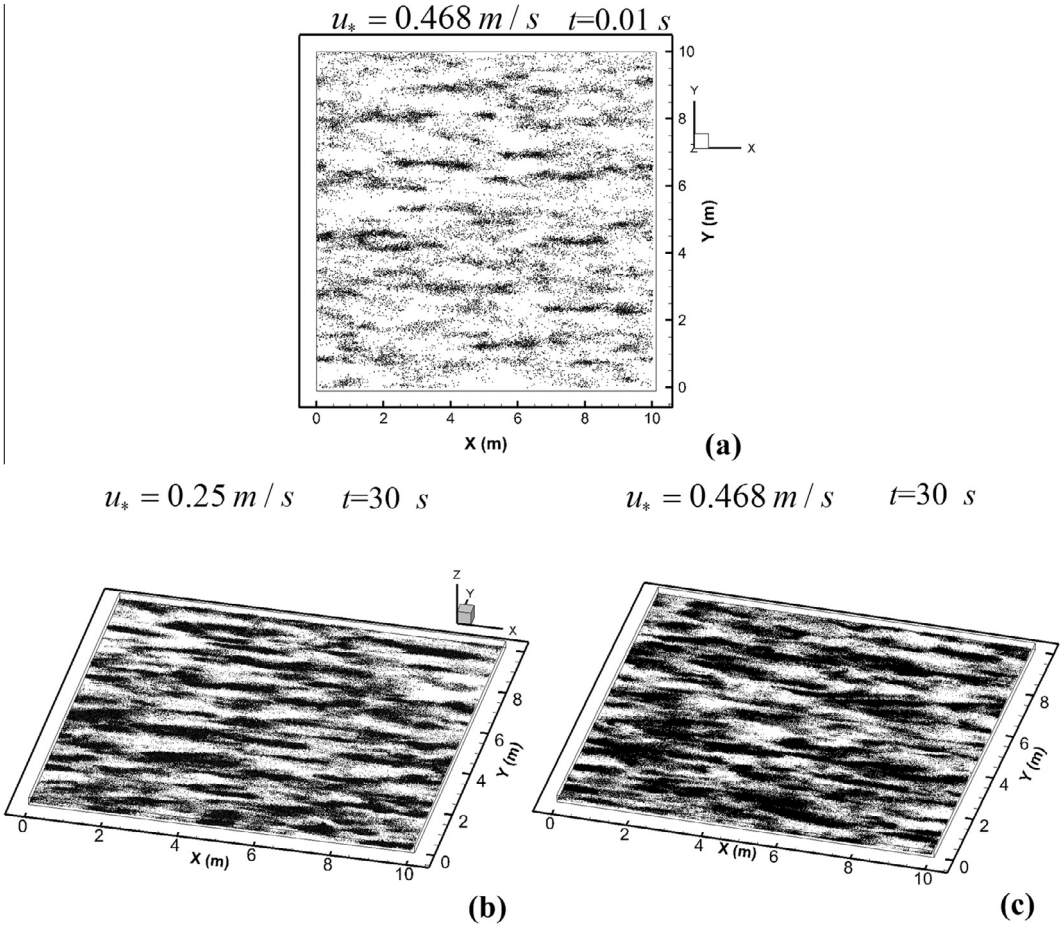

Fig. 5. The blown snow structure under different friction velocities after 30 s development of drifting snow (one dark spot stands for a snow particle).

Baas, 2008). Baas and Sherman (2005) divided the aeolian streamers into three patterns: the streamer families, nested streamers and clouds with embedded streamers. Different types of streamers can be distinguished by the spanwise averaged transport intensity μ_y and spanwise standard variance σ_y of the transport intensity I. Normalize the transport intensity by μ_y, the spanwise standard deviations σ_y under friction velocities of 0.25 ms^{-1}, 0.302 ms^{-1}, 0.411 ms^{-1} and 0.468 ms^{-1} are 1.731, 1.712, 1.672 and 1.667, respectively. So the snow streamers belong to streamer families under these wind speeds. At the same time, σ_y decreases slowly with increasing friction velocity and is still larger than μ_y when the friction velocity is 0.85 ms^{-1} in our simulation. Thus other streamer patterns of snow may appear later compared to that of drifting sand. This is mainly because the follow performance of snow particles is much better than that of sand grains and thus saltation snow is easier to be dominated by turbulent flow.

Use the same threshold $\mu_y + \sigma_y$ to determine the outline of snow streamer, the characteristic scales of snow streamers can be obtained. Here, we first find out all streamers in the computational domain based on a position correlation method. The position correlation method can be described as follow: if the transport intensity I in a statistical unit is larger than the threshold and this point has at least one adjacent point that belongs to an identified streamer, this cell will be assigned to be part of the streamer. Fig. 6 is the effect of the identified snow streamers with the position correlation method. It can be observed that this method has a good recognition performance. Then the identified streamers will be numbered and their sizes can be acquired accordingly.

As illustrated in Fig. 7, the probability distributions of the characteristic sizes of snow streamers are given, in which (a) is the characteristic width, (b) is the characteristic length, (c) is the lateral spacing and (d) is the projected area. It can be seen that the size of snow streamers are not sensitive to the wind speed basically. The mean values of various characteristic parameters under different friction velocities are shown in Table 1, in which the projected area is the shaded area in Fig. 6, the number means the mean number of streamers in one square meters of space, and the coverage rate is defined as the area of streamers to the total area. Seen from Table 1, snow streamers have a mean characteristic length of around 0.5 m and an average spanwise width of about 0.16 m. On average, there are 1.4 independent snow streamers within one square meter and the spanwise space between two adjacent streamers is about 1.3 m. And about 9% of the ground surface is covered by snow streamers during drifting snow.

Baas and Sherman (2005) observed that the typical sand streamers display a characteristic width of approximately 0.2 m and an average lateral spacing of about 1 m. These values are almost consistent with our simulation results. The width of snow streamers is slight smaller than that of the sand streamers mainly because the sand particles have stronger inertia compared to that of snow grains, which may lead to the worse aggregation of sand particles in the process of stochastic grain-bed interactions.

3.3. The formation of snow streamers

The formation mechanism of sand streamers has been investigated based on the field observation and theoretical analysis (Baas and Sherman, 2005; Baas, 2008). Generally, the transport variability of blown sand is contributed by spatial and temporal variations in both the airflow and the bed surface control, in which the surface control includes moisture content, grain size, and microtopography etc. The analysis on snow streamers also concentrates on these two aspects.

The turbulence is composed of plenty of vortexes with different sizes and shapes, in which the vortex can be interpreted as the local fluids swirling around the vortex core (Robinson, 1991). The results of Baas and Sherman (2005) showed weak correlation between streamwise vortices and aeolian streamers. The same is true for drifting snow if the rotation intensity of vortexes is indiscriminate. Fig. 8(a) shows the vortex structure ($\Omega = 0.52$) in the fully developed turbulent boundary layer with the omega vortex identification method (Liu et al., 2016), where Ω is defined as the vortical vorticity over the total vorticity. Here, the total vorticity is expressed as the curl of velocity and the vortical vorticity is denoted as a, which is the vortical part of the vortex and can be expressed as (Liu et al., 2016):

$$a = [(\partial u_1/\partial x_2 - \partial u_2/\partial x_1)^2 + (\partial u_1/\partial x_3 - \partial u_3/\partial x_1)^2 + (\partial u_2/\partial x_3 - \partial u_3/\partial x_2)^2]/4 \quad (12)$$

It can be seen that the turbulent vortices are basically evenly distributed in the boundary layer and it is hard to find the corresponding relation between the distributions of vortexes and particle concentrations.

However, since a rotating vortex is just worked as a 'tornado', snow particles may get into the vortexes and the intensity of the vortexes should be directly related to this process. We use the vortical vorticity (a) of the vortex to describe the rotation intensity of the vortex. Fig. 8(b) gives the distributions of vortical vorticity larger than 2000 (s^{-2}) and saltating snow particles, in which the green patches are vortical vorticities and the black points represent snow particles. It can be seen from this figure that the high concentration snow streamers are basically located in the high-speed rotating vortexes. Thus the formation of snow streamers in the turbulent boundary layer should be mainly contributed by local rotational motion of fluid. While the research of Baas and Sherman (2005) indicate that the near-surface gusts could be the main reason that forms the sand streamers. The major reasons may be that the rotation intensity of the turbulent vortexes is omitted in their analysis.

In order to quantitatively demonstrate the corresponding relation between the particle concentration and rotational speed of local vortex, the variation of mean vortical vorticity $\bar{a}$ with particle

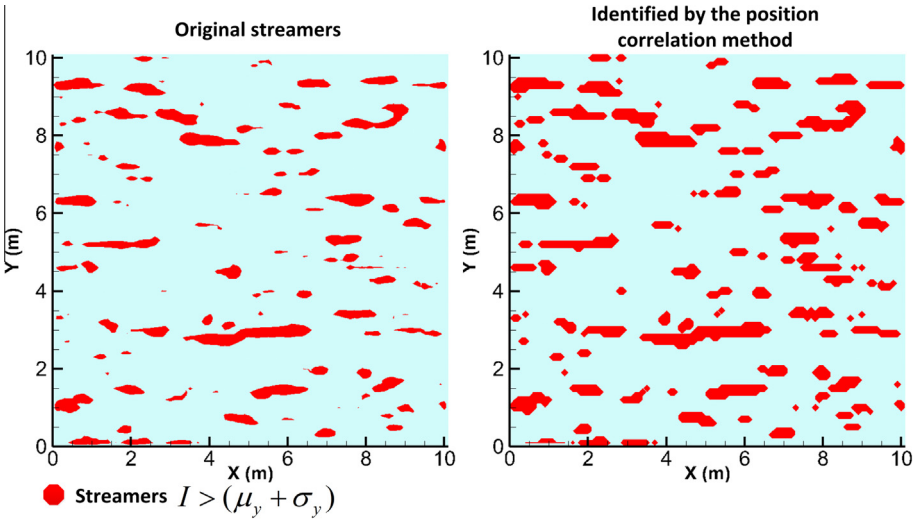

Fig. 6. The snow streamers identified by the position correlation method.

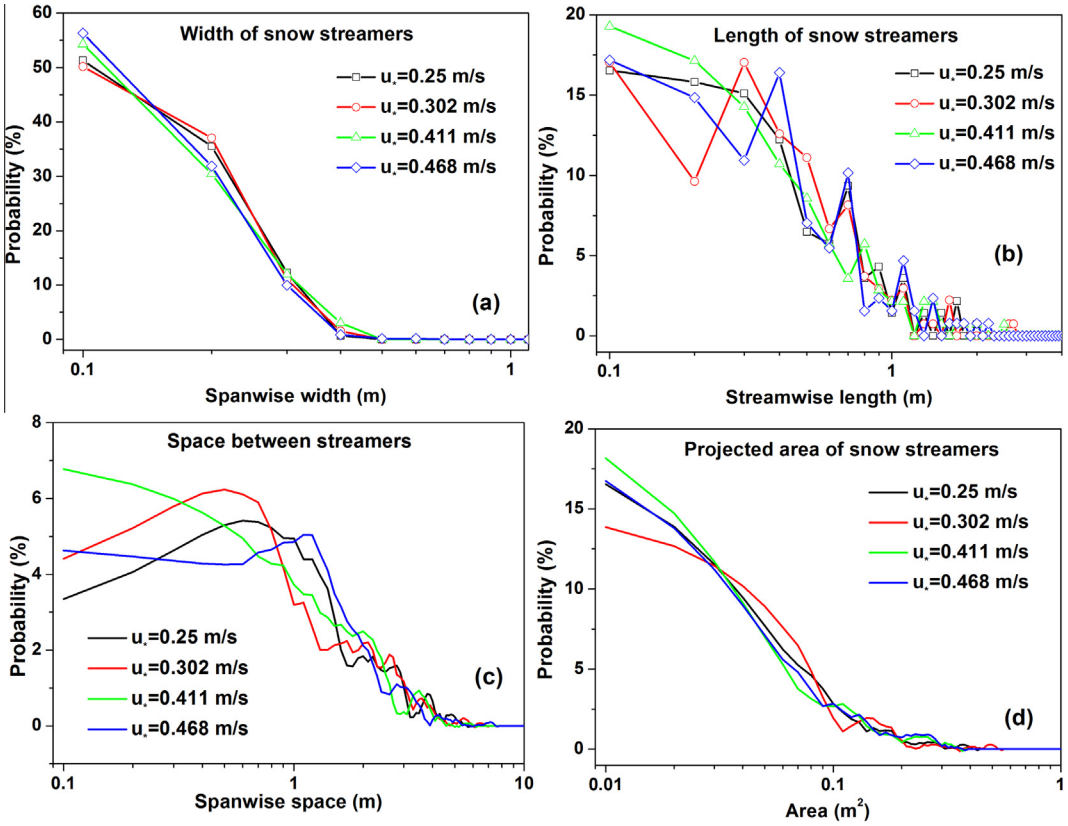

Fig. 7. The probability distributions of the characteristic sizes of snow streamers under different friction velocities.

Table 1
The mean values of different characteristic parameters of snow streamers under different friction velocities.

Friction velocity (ms^{-1})	Mean spanwise width (m)	Mean streamwise length (m)	Mean lateral spacing (m)	Mean projected area (m^2)	Number (m^{-2})	Coverage rate (–)
0.25	0.164	0.509	1.385	0.0713	1.28	0.088
0.302	0.164	0.484	1.402	0.0678	1.4	0.091
0.411	0.163	0.51	1.261	0.0716	1.35	0.093
0.468	0.162	0.488	1.37	0.069	1.39	0.089

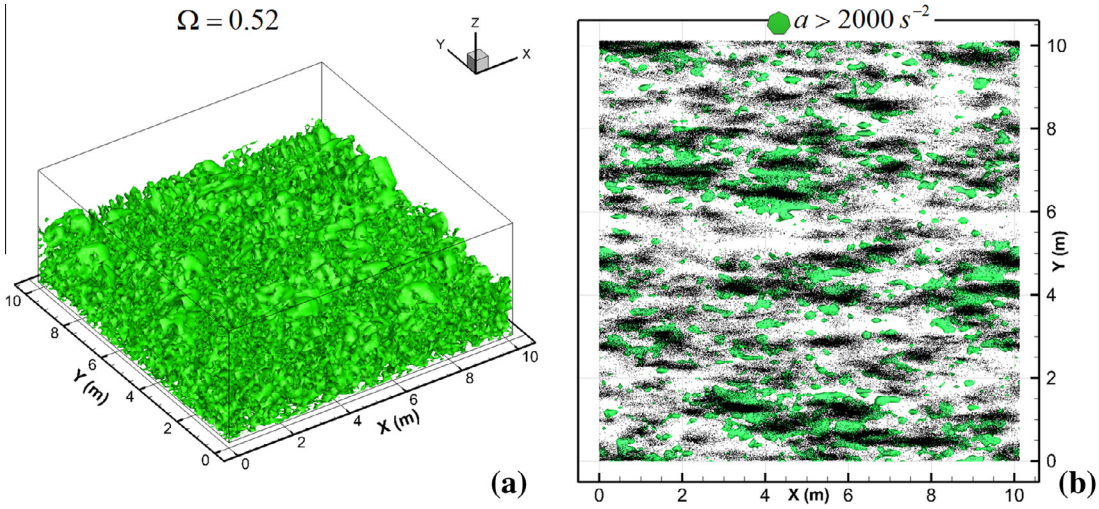

Fig. 8. (a) The vortex structure in the turbulent boundary layer and (b) the distributions of vortical vorticities larger than 2000 (s^{-2}) and saltating snow particles after 30 s development of drifting snow ($u_* = 0.468$ m/s and one dark spot stands for a snow particle).

concentration in a fully developed drifting snow under friction velocity of 0.35 ms^{-1} is displayed in Fig. 9. The particle concentration has been normalized by the mean concentration of particles and the horizontal slice of the vortical vorticity a at a height of mean saltation height (1.31 cm) was used to obtain the local vortical vorticity. It can be obviously found that particle concentration is proportional to the rotational speed of local vortex. The mean value of the local vortical vorticity is basically exponential increase with the increase of particle concentration. The reason is mainly because vortexes with higher rotational speeds could generate a much stronger suction and absorb more saltating snow particles.

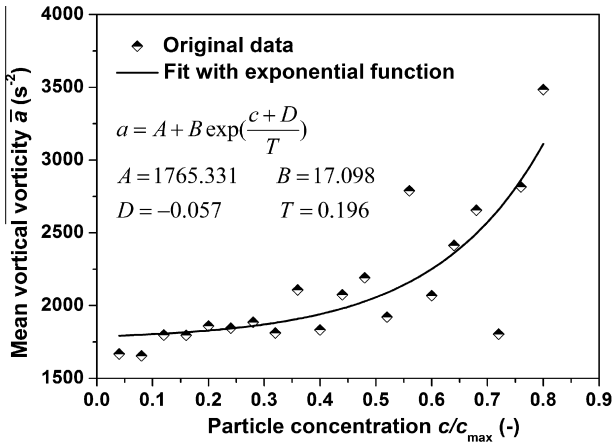

Fig. 9. The correlation between particle concentrations and local vortical vorticity.

Further study shows that the snow streamers are largely self-organized by turbulent vortexes and the effect of spatial differentiation of particle entrainment may not significant in this process. This is also consistent with the observation of Baas and Sherman (2005) that the surface control was not a necessary condition for the formation of aeolian streamers. Fig. 10 gives different streamers patterns after 30 s development of drifting snow in the turbulent boundary layer under various grain-bed interactions. The initial state is a uniform distributed saltating snow particles, in which the particles only conduct a rebound with mirror reflection condition for case (a), case (b) is just as (a) except that the rebound particles have a stochastic horizontal angle towards the impacting direction ($\sigma(\beta_{hor}) = 10^{\circ}$), and case (c) processes a normal grain-bed interaction described in the model and method. Fig. 10(a), (b) and (c) are the planforms of saltating snow particles after 30 s development of drifting snow.

It can be observed that the final shape of the snow streamers is largely related to the stochastic grain-bed interactions of snow particles. Generally, the deviation from the incident direction of snow particles during the impacting process (case b) extend the width of streamers or even merge the adjacent streamers, and the newly ejected particles will lengthen the length of the streamers (case

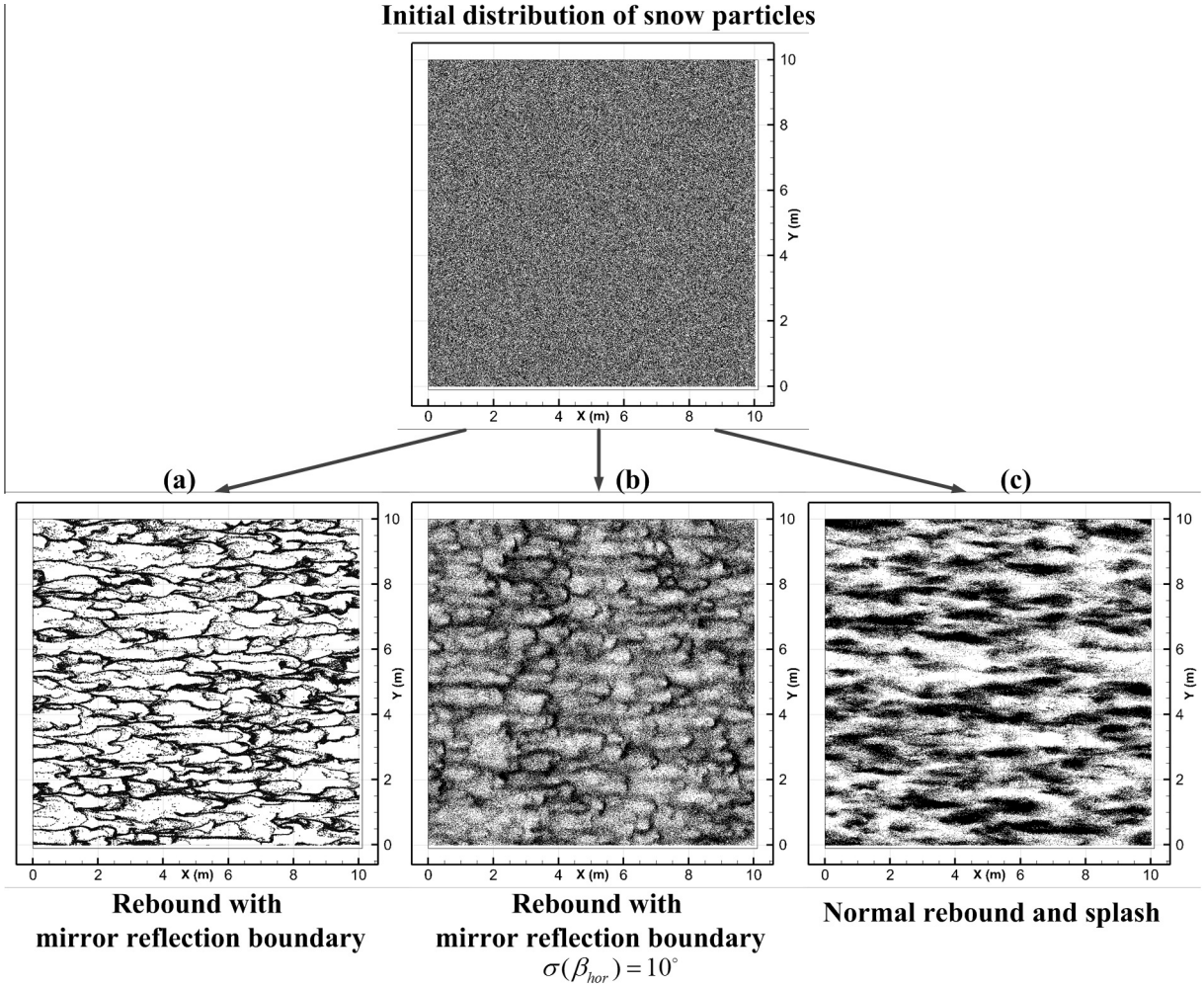

Fig. 10. The different types of snow streamers with different grain-bed interactions ($u_* = 0.25$ ms^{-1} and one dark spot stands for a snow particle).

c). The characteristic length and width of snow streamer (case c in Fig. 10) are 0.496 m and 0.163 m, respectively. This is consistent with the characteristic size of streamers that formed by the normal entrainment and splash process (Fig. 5a). Thus the formation of snow streamers is independent of the spatial differentiation of particle entrainment. Further results also show that the magnitude of the deviation angle β_{hor} does not affect the characteristic size of snow streamers, which also indicates that the snow streamer is basically a self-organization phenomenon of mid-air snow particles driven by the turbulent vortexes.

Based on the above analysis, the snow streamers are high concentration particle clouds that organized by the high-speed rotating vortexes in the turbulent boundary layer. And the final shape and distribution of snow streamers is generated by the combined action of turbulent vortex and random grain-bed interaction.

4. Conclusions

In this study, a 3-D drifting snow model with mixed particle size in the turbulent boundary layer is established through tracking every saltation particle with explicit consideration of the coupling effect between snow particles and airflow. The snow streamers are reproduced in the turbulent boundary layer. For snow streamers, the transition from streamer families to nested streamers or other more complex streamer patterns generally needs a much larger wind speed than that of sand due to the good following performance of snow particles.

The characteristic sizes of snow streamers are analyzed based on a position correlation method. The mean characteristic length and width of snow streamers are approximately 0.5 m and 0.16 m, respectively. The average coverage rate of snow streamers during drifting snow is about 9% and it is constant under different wind speeds. On average, one square meter of space contains 1.4 independent streamers and their lateral spacing is around 1.3 m. All these characteristic parameters are not sensitive to the wind speed.

The rotation speed of the turbulent vortexes is found to be directly related to the formation of snow streamers. That is, high-speed rotating vortexes can trap the saltating snow particles like a ‘tornado’. Statistical results show a good correlation between local particle concentration and rotation speed of the vortex. The spatial non-uniform aerodynamic entrainment has no obvious effect on snow streamers, but the grain-bed interactions have important influence on the final shape of snow streamers.

Acknowledgements

This work is supported by the State Key Program of National Natural Science Foundation of China (91325203), the National Natural Science Foundation of China (41371034), the Innovative Research Group of the National Natural Science Foundation of China (Grant No. 11421062), the Fundamental Research Funds for the Central Universities (lzujbky-2015-237), and the Fundamental Research Funds for the Central Universities (862166).

Appendix A. Supplementary data

Supplementary data associated with this article can be found, in the online version, at http://dx.doi.org/10.1016/j.aeolia.2016.09.002.

References

Anderson, R.S., Haff, P.K., 1988. Simulation of eolian saltation. Science 241, 820–823.
Anderson, R.S., Haff, P.K., 1991. Wind modification and bed response during saltation of sand in air. Acta Mech. 1, 21–51.
Baas, A.C.W., 2008. Challenges in aeolian geomorphology: investigating aeolian streamers. Geomorphology 93, 3–16.
Baas, A.C.W., Sherman, D.J., 2005. Formation and behavior of aeolian streamers. J. Geophys. Res. 110, F03011.
Bagnold, R.A., 1973. The Physics of Blown Sand and Desert Dunes. Chapman and Hall, London.
Bintanja, R., 2000a. Snowdrift suspension and atmospheric turbulence. Part I: Theoretical background and model description. Boundary Layer Meteorol. 95 (3), 343–368.
Bintanja, R., 2000b. Snowdrift suspension and atmospheric turbulence. Part II: Results of Model Simulations. Boundary Layer Meteorol. 95 (3), 369–395.
Déry, S., Yau, M.K., 1999. A bulk blowing snow model boundary-layer. Meteorology 93 (2), 237–251.
Dupont, S., Bergametti, G., Marticorena, B., Simoëns, S., 2013. Modeling saltation intermittency. J. Geophys. Res. 118 (13), 7109–7128.
Fukushima, Y., Etoh, T., Ishiguro, S., Kosugi, K., Sato, T., 2001. Fluid dynamic analysis of snow drift using a non-Boussinesq k-ε turbulence model (in Japanese with English abstract). Seppyo 63, 373–383.
Fukushima, Y., Fujita, K., Suzuki, T., Kosugi, K., Sato, T., 1999. Flow analysis of developing snowdrifts using a k-ε turbulence model (in Japanese with English abstract). Seppyo 61, 285–296.
Gallée, H., Trouvilliez, A., Agosta, C., Genthon, C., Favier, V., Naaim-Bouvet, F., 2013. Transport of snow by the wind: a comparison between observations in Adélie Land, Antarctica, and simulations made with the regional climate model MAR. Boundary Layer Meteorol. 146, 133–147.
Gauer, P., 2001. Numerical modeling of blowing and drifting snow in Alpine terrain. J. Glaciol. 47 (156), 97–110.
Gordon, M., Taylor, P.A., 2009. Measurements of blowing snow, Part I: Particle shape, size distribution, velocity, and number flux at Churchill, Manitoba, Canada. Cold Reg. Sci. Technol. 55, 63–74.
Gromke, C., Horender, S., Walter, B., Lehning, M., 2014. Snow particle characteristics in the saltation layer. J. Glaciol. 60, 431–439.
Groot Zwaaftink, C.D., Diebold, M., Horender, S., Overney, J., Lieberherr, G., Parlange, M., Lehning, M., 2014. Modelling small-scale drifting snow with a Lagrangian stochastic model based on large-eddy simulations. Boundary Layer Meteorol. 153, 117–139.
Huang, N., Wang, Z.S., 2015. A 3-D simulation of drifting snow in the turbulent boundary layer. Cryosphere Discuss. 9, 301–331.
Kok, J.F., Renno, N.O., 2009. A comprehensive numerical model of steady state saltation (COMSALT). J. Geophys. Res. 114 (D17), D17204.
Lehning, M., Löwe, H., Ryser, M., Raderschall, N., 2008. Inhomogeneous precipitation distribution and snow transport in steep terrain. Water Resour. Res. 44, W07404.
Li, W., Zhou, Y., 2007. Statistical behaviors of different-sized grains lifting off in stochastic collisions between mixed sand grains and the bed in aeolian saltation. J. Geophys. Res. 112, D22206.
Liu, C.Q., Wang, Y.Q., Yang, Y., Duan, Z.W., 2016. New omega vortex identification method. Sci. China Phys. Mech. Astron. 59, 684711.
Lund, T.S., Wu, X., Squire, K.D., 1998. Generation of turbulent inflow data for spatially-developing boundary layer simulations. J. Comput. Phys. 140 (2), 233–258.
Mann, G.W., Anderson, P.S., Mobbs, S.D., 2000. Profile measurements of blowing snow at Halley. Antarctica. J. Geophys. Res. 105, 24491–24508.
Meneveau, C., Lund, T., Cabot, W., 1996. A Lagrangian dynamic subgrid-scale model of turbulence. J. Fluid Mech. 319, 353–385.
Michaux, J.L., Naaim-Bouvet, F., Naaim, M., 2001. Drifting-snow studies over an instrumented mountainous site: II. Measurements and numerical model at small scale. Ann. Glaciol. 32 (1), 175–181.
Nemoto, M., Nishimura, K., 2004. Numerical simulation of snow saltation and suspension in a turbulent boundary layer. J. Geophys. Res. 109, D18206.
Nishimura, K., Yokoyama, C., Ito, Y., Nemoto, M., Naaim-Bouvet, F., Bellot, H., Fujita, K., 2014. Snow particle speeds in drifting snow. J. Geophys. Res. Atmos. 119 (16), 9901–9913.
Omiya, S., Sato, A., Kosugi, K., Mochizuki, S., 2011. Estimation of the electrostatic charge of individual blowing-snow particles by wind tunnel experiment. Ann. Glaciol. 52 (58), 148–152.
Okaze, T., Mochida, A., Tominaga, Y., Nemoto, M., Sato, T., Sasaki, Y., Ichinohe, K., 2012. Wind tunnel investigation of drifting snow development in a boundary layer. J. Wind Eng. Ind. Aerodyn. 104 (106), 532–539.
Rice, M.A., Willetts, B.B., McEwan, I.K., 1995. An experimental study of multiple grain-size ejection produced by collisions of saltating grains with a flat bed. Sedimentology 42 (4), 695–706.
Robinson, S.K., 1991. Coherent motions in the turbulent boundary layer. Annu. Rev. Fluid Mech. 23, 601–639.
Schmidt, R.A., 1984. Measuring particle size and snowfall intensity in drifting snow. Cold Reg. Sci. Technol. 9 (2), 121–129.
Schneiderbauer, S., Prokop, A., 2011. The atmospheric snow-transport model: SnowDrift3D. J. Glaciol. 52 (203), 526–542.
Smagorinsky, J., 1963. General circulation experiments with the primitive equations: I. The basic experiment. Mon. Weather Rev. 91 (3), 99–164.
Sugiura, K., Nishimura, K., Maeno, N., Kimura, T., 1998. Measurements of snow mass flux and transport rate at different particle diameters in drifting snow. Cold Reg. Sci. Technol. 27 (2), 83–89.
Taylor, P., 1998. The thermodynamic effects of sublimating, blowing snow in the atmospheric boundary layer. Boundary Layer Meteorol. 89 (2), 251–283.

Tominaga, Y., Okaze, T., Mochida, A., Sasaki, Y., Nemoto, M., Sato, T., 2013. PIV measurements of saltating snow particle velocity in a boundary layer developed in a wind tunnel. J. Visualization 16 (2), 95–98.
Uematsu, T., Nakata, T., Takeuchi, K., Arisawa, Y., Kaneda, Y., 1991. Three-dimensional numerical simulation of snowdrift. Cold Reg. Sci. Technol. 20 (1), 65–73.
Urbin, G., Knight, D., 2001. Large-Eddy simulation of a supersonic boundary layer using an unstructured grid. AIAA J. 39 (7), 1288–1295.
Vinkovic, I., Aguirre, C., Ayrault, M., Simoëns, S., 2006. Large-eddy simulation of the dispersion of solid particles in a turbulent boundary layer. Boundary Layer Meteorol. 121 (2), 283–311.
Vionnet, V., Martin, E., Masson, V., Guyomarc'h, G., Naaim-Bouvet, F., Prokop, A., Durand, Y., Lac, C., 2014. Simulation of wind-induced snow transport and sublimation in alpine terrain using a fully coupled snowpack/atmosphere model. Cryosphere 8, 395–415.
Xiao, J., Bintanja, R., Déry, S., Mann, G., Taylor, P., 2000. An intercomparison among four models of blowing snow. Boundary Layer Meteorol. 97 (1), 109–135.
Xue, M., Droegemeier, K.K., Wong, V., 2000. The advanced regional prediction system (ARPS)-A multiscale nonhydrostatic atmospheric simulation and prediction model. Part I: model dynamics and verification. Meteorol. Atmos. Phys. 75, 161–193.
Xue, M., Droegemeier, K.K., Wong, V., Shapiro, A., Brewster, K., Carr, F., Weber, D., Liu, Y., Wang, D., 2001. The Advanced regional prediction system (ARPS)-A multi-scale nonhydrostatic atmospheric simulation and prediction tool. Part II: model physics and applications. Meteorol. Atmos. Phys. 76, 143–165.
Zhang, J., Huang, N., 2008. Simulation of snow drift and the effects of snow particles on wind. Modell. Simul. Eng., 408075–408076
Zhou, J., Pomeroy, J.W., Zhang, W., Cheng, G., Wang, G., Chen, C., 2014. Simulating cold regions hydrological processes using a modular model in the west of China. J. Hydrol. 509, 13–24.